Efficient Charging of Supercapacitors for Extended Lifetime of Wireless Sensor Nodes

Farhan I. Simjee, *Member, IEEE*, and Pai H. Chou, *Member, IEEE*

***Abstract*—This paper describes an efficient charging method for a supercapacitor-operated, solar-powered wireless sensor node called Everlast. Unlike traditional wireless sensors that store energy in batteries, Everlast's use of supercapacitors enables the system to operate for an estimated lifetime of 20 years without any maintenance. The novelty of this system lies in the feed-forward, pulse frequency modulated converter and open-circuit solar voltage method for maximum power point tracking (MPPT), enabling the solar cell to efficiently charge the supercapacitor and power the node. Experimental results show that by its low-complexity MPPT, Everlast can achieve over 89% conversion efficiency with lower power overhead than the state-of-the-art by two orders of magnitude, while enabling charging a supercapacitor up to 400% faster than direct charging. This makes Everlast particularly applicable to miniature-scale, high-impedance energy harvesting systems.**

***Index Terms*—Energy harvesting, maximum power point tracking (MPPT), solar power, supercapacitor, wireless sensor node (WSN).**

I. Introduction

LONG-TERM operation is an important goal of many wireless sensor network (WSN) systems. One may attempt to achieve this goal three ways: reduce energy consumption of the system, increase energy capacity of the battery, and replenish battery energy over time. Energy reduction can be done by improving hardware design and more intelligent power management, which entails turning off unused components or slowing down during idle periods. Unfortunately, batteries are limited by both their energy capacities as well as their number of recharge cycles, even if the system already consumes very low power. As a result, it is necessary to not only harvest energy efficiently from the environment, but also store the energy in a medium that has much more longevity than batteries.

A. Batteries versus Supercapacitors

Many of today's WSNs rely on batteries as the primary power source. Batteries are frequently cited as the primary limiting factor in the lifetime of these WSNs. Due to the limited number of recharge cycles and inability to hold full charge for long periods of time, the battery will require replacement after one to two years. Unfortunately, such recurring maintenance cost is likely to become very expensive or prohibitive if it must be done for thousands of deeply embedded nodes, which are likely to be difficult or expensive to access after deployment. In both cases above, the battery is the primary limiting factor that prevents the node from operating maintenance-free for more than several years at non-trivial data rates.

By removing the battery altogether and storing energy solely in the supercapacitor, there is now a viable option for achieving even longer life operation. Supercapacitors have received wide attention recently due to their power density, low equivalent series resistance (ESR), and lower leakage current than electrolytics [1]. Table I compares batteries and supercapacitors available for wireless sensor applications. The supercapacitor offers more than half a million charge cycles and a 10-year operational lifetime before the energy capacity is reduced to 80% and internal resistance is doubled, which is the point where half the original capacity is available for a supercapacitor or battery at rated current. The supercapacitor generally has an order of magnitude higher continuous current than a battery, and so when a supercapacitor's capacity falls down to 80% and internal resistance doubles, nearly 80% of the original capacity can still be drained as long as the sensor node's peak current is less than a tenth of the supercapacitor's continuous current. Continuous current for the Maxwell 350 F is greater than 80 A, and so when the sensor node draws less than 8 A peak current, most of the remaining capacity can be utilized. The supercapacitor is estimated to take 20 years to reach 50% capacity degradation. Fig. 1 shows the energy quota for the different types of energy storage listed above.

B. Maximum Power Point Tracking (MPPT) for Small Devices

Maximum power point tracking (MPPT) is the problem of determining the optimal load based on the condition of the energy harvesting device. Unlike regulated power supplies and most batteries whose impedance values remain $<1\ \Omega$, many energy harvesting devices including solar panels, piezoelectric generators, and even windmills have relatively high impedance on the order of several hundred to tens of thousands of ohms, and it is a function of the power before conversion, the load, and temperature.

For large energy harvesting devices, the goal of MPPT should be to maximize the transfer efficiency, whereas for smaller devices, the goal should be to minimize the MPPT overhead. This is because for large-scale devices that output hundreds or thousands of watts of power, even a one-percent efficiency loss can

Manuscript received December 27, 2006; revised September 3, 2007. An earlier version of this paper appeared in the International Symposium on Low Power Electronics and Design (ISLPED), Tegernsee, Germany, October 4–6, 2006. This work was supported in part by NSF Grant CCR-0205712 and NSF CAREER Award CNS-0448668. Recommended for publication by Associate Editor K. Ngo.

F. I. Simjee is with the European Aeronautic Defence and Space Company (EADS), Schiphol-Rijk, The Netherlands (e-mail: fsimjee@alumni.uci.edu).

P. H. Chou is with the University of California, Irvine, CA 92697 USA and also with National Tsing Hua University, Hsinchu 300, Taiwan, R.O.C.

Digital Object Identifier 10.1109/TPEL.2008.921078

TABLE I
ENERGY STORAGE TECHNOLOGIES AVAILABLE FOR SENSOR NODES

Maxwell BCAP350	Panasonic HHR210AA/B	Panasonic CGR17500	Maxwell PC10	Panasonic BR-AG	
350F Supercap.	NiMH	Lithium-Ion	10F Supercap.	Lithium	**Storage Type**
500,000	300	500	500,000	0	**Full Charge Cycles**
243	2,000	830	6.9	2,200	**Capacity (mAh)**
2.5	1.2	3.6	2.5	3.0	**Nominal Voltage (V)**
87,500	2,000	830	2,500	2.5	$I_{cont,initial}$ **(mA)**
10-20yrs	<3 yrs	<5 yrs	10-20yrs	≈10-20 yrs	**Lifetime (at 25°C)**
D size	AA size	AA size	29.6 x 23.6 x 4.8	AA size	**Dimensions (mm)**
≈$20	≈$3	≈$10	≈$10	≈$10	**Cost @ qty. 10**
60g	29g	25g	6.3g	18g	**Weight (g)**
−40 to 65°C	−10 to 65°C	−20 to 60°C	−40 to 70°C	−40 to 85°C	**Operating temp.**
1,100J	7000J @ 80% DoD	1,075J @ 10% DoD	31.25J	<3J	E_{max} **/ day Initial**
<1 mA, <30%/month	<30%/month	<10%/month	<0.04mA, <30%/month	<1%/month	**Self-discharge Rate**

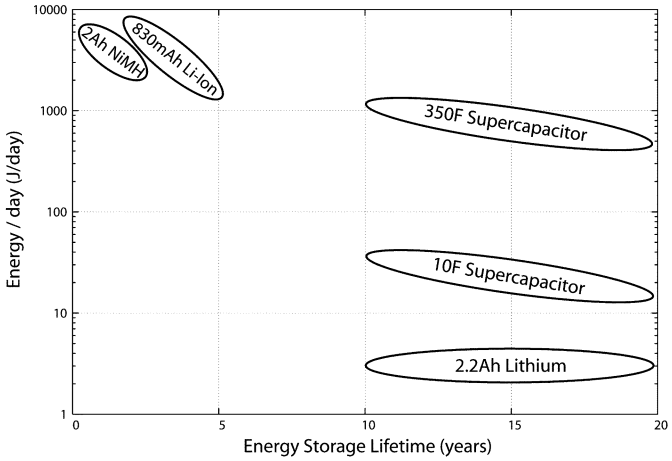

Fig. 1. Daily maximum energy quotas for energy storage types in Table I.

be large. The MPPT overhead, although somewhat computationally intensive, would consume several hundred milliwatts of power, but it is a small fraction of the output of a large solar panel. On the other hand, wireless sensor nodes cannot afford to spend several hundred milliwatts of power on MPPT, because that would be 1–2 orders of magnitude higher than the peak power consumption of a sensor node itself. In fact, a smaller solar panel may not even be able to output enough power for such an MPPT controller. Therefore, an MPPT controller for small devices must maximize net power transfer mainly by minimizing MPPT overhead, while it can afford to sacrifice MPPT accuracy.

C. MPPT While Charging Supercapacitors

Discrete capacitors are always in supply rails for decoupling purposes and are usually attached straight to the power source. Since the values are in the micro-farad (μF) range, they charge up very quickly. If a capacitor that is in the hundreds of farads is attached to the power source, the component acts as a short and the supply rail voltage drops to the capacitor voltage. The same situation occurs when a large capacitor is attached directly to a solar cell. Although the solar cell will charge under this condition, it will not do so efficiently, because it will not be at the maximum power point (MPP), the voltage and current combination that maximizes power output under a given sunlight condition. A supercapacitor has been charged in this manner before but this reduces the solar efficiency by a factor of 2-5$\times$ depending on the solar cell topology [2].

Charger ICs require a minimum of 10 mA to operate and would be inefficient. Typical voltage regulator ICs may consume as little as 20–100 μA, but they are not suitable for charging the supercapacitor. This is because the feedback voltage will signal to the regulator that the output voltage is too low and short the input to the output similar to the situation described above. For this reason, pulse power applications use resonant converters and the Ward converter to efficiently and quickly charge capacitors [3], [4]. Unfortunately, this particular resonant converter requires an ac voltage that cannot be generated by the solar panel. The Ward converter inputs dc power, but the circuit is rather complex and requires a low impedance power source such as a battery or electrical outlet. Clearly, a new converter design is needed to meet the requirement of efficiently charging a low impedance capacitor from a high impedance power source such as a solar cell, wind generator, or piezoelectric generator.

D. Contributions

The purpose of this work is to demonstrate the feasibility of such a sensor node operating on supercapacitors recharged by solar cells. One could not simply replace a battery with a

supercapacitor because of the very different electrical characteristics and efficiency considerations in relation to the solar cells. We propose a feed-forward, pulse frequency modulated regulator that charges the supercapacitor at near optimal operating points for solar cells. We have constructed a complete wireless sensor node called Everlast with this solar/supercapacitor power circuitry and stress-tested its operation. Experimental results show that the Everlast node can achieve low power consumption, long operational lifetime, and high transmission rates simultaneously, without forcing the user to make trade-offs. This is expected to enable a whole new class of applications for low-cost, high performance, durable wireless sensor networks.

The proposed circuitry has a wide range of applications. The most obvious ones are those that deploy sensor nodes in remote locations where long operational lifetimes are critical, particularly in the area of environmental and structural sensing. Installation labor costs in remote habitats and buildings far exceed the cost of the actual node and so increasing the time between node replacements will make it economically feasible to install sensor nodes in remote locations. Our circuitry is not exclusive to solar panels; it is applicable to many other devices that harvest energy from high-impedance supplies and store energy capacitively. For example, although medical implants typically do not get solar power, they can harvest energy from vibration of the body and charge the supercapacitor using the regulator described in this work. A hybrid primary battery/supercapacitor energy source would decrease battery drain and allow the device lifetime to reach the 10 year shelf life of the battery, instead of 1–5 years currently.

II. Background and Related Work

Charging a capacitor and drawing maximum solar power are both areas of active research. However, the authors are not aware of prior work on efficiently charging a capacitor using optimal solar power. The problem is to build a power converter that can very efficiently charge a large capacitor while keeping the solar cell at the optimal voltage and current. Since the goal is to reduce the complexity of the circuit as much as possible, the solution will need to trade off the cost/complexity of the power converter with efficiency and the cost/complexity of the MPPT circuitry with accuracy. This section reviews characteristics of solar panels, followed by a review of MPPT techniques.

A. MPP in Solar Panels

To formulate the MPP problem, we define the following variables:

E	plane-of-array solar irradiance ($\mathrm{W/m^2}$);
E_e	effective irradiance, or "suns;"
AM_a	absolute air mass (dimensionless);
AOI	solar angle-of-incidence on module (degrees);
T_c, T_o	temperature of cells and reference temperature (°C);
$I_{\mathrm{sco}}, I_{\mathrm{mpo}}$	ref. short-circuit current and ref. max. power current;
$V_{\mathrm{oco}}, V_{\mathrm{mpo}}$	ref. open-circuit voltage and ref. max. power voltage;
$\alpha_{I_{\mathrm{sc}}}, \alpha_{I_{\mathrm{mp}}}, \beta_{V_{\mathrm{oc}}}, \beta_{V_{\mathrm{mp}}}$	temperature coefficients;
$C_0 - C_4$	empirical coefficients;
$K_{I_{\mathrm{mp}}}, K_{V_{\mathrm{mp}}}$	constants to calculate I_{mp} and V_{mp} from I_{sc} and V_{oc}.

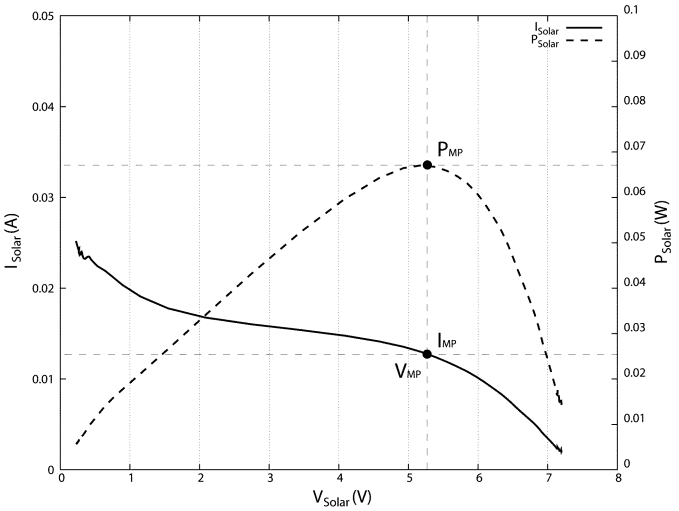

Fig. 2. Solar cell I–V curve- maximum power generated at P_{mp}.

The following equations characterize solar panels in terms of short-circuit current and effective irradiance:

$$I_{\mathrm{sc}}(E, T_c, \mathrm{AM}_a, \mathrm{AOI}) = (E/E_o) f_1(\mathrm{AM}_a) f_2(\mathrm{AOI}) \cdot (I_{\mathrm{sco}} + \alpha_{I_{\mathrm{sc}}}(T_c - T_o)) \quad (1)$$

$$E_e = \frac{I_{\mathrm{sc}}(E, T_c = T_o, \mathrm{AM}_a, \mathrm{AOI})}{I_{\mathrm{sco}}}. \quad (2)$$

The maximum power current, open-circuit voltage, and maximum power voltage are given as

$$I_{\mathrm{mp}}(E_e, T_c) = C_0 + E_e(C_1 + \alpha_{I_{\mathrm{mp}}}(T_c - T_o)) \quad (3)$$

$$V_{\mathrm{oc}}(E_e, T_c) = V_{\mathrm{oco}} + C_2 \ln(E_e) + \beta_{V_{\mathrm{oc}}}(T_c - T_o) \quad (4)$$

$$V_{\mathrm{mp}}(E_e, T_c) = V_{\mathrm{mpo}} + C_3 \ln(E_e) + C_4(\ln(E_e))^2 + \beta_{V_{\mathrm{mp}}}(T_c - T_o). \quad (5)$$

The maximum power described in (3) and (5) is directly dependent upon the solar intensity and the temperature [5]. Under a given sunlight condition, the solar power output is maximized when the following (6) holds:

$$\frac{dP_{\mathrm{solar}}}{dV_{\mathrm{solar}}} = \frac{dP_{\mathrm{solar}}}{dI_{\mathrm{solar}}} = 0. \quad (6)$$

This peak solar power output is further illustrated in Fig. 2 where for a given instance an ideal operating voltage and current exist. The figure also reveals that pinpoint accuracy is not necessary. Within a $\pm 5\%$ deviation of the operating voltage from V_{mp} the solar cell can generate close to 95% of the peak power. This provides enough flexibility in the implementation of the MPP tracker as to reduce the cost and complexity of the circuitry.

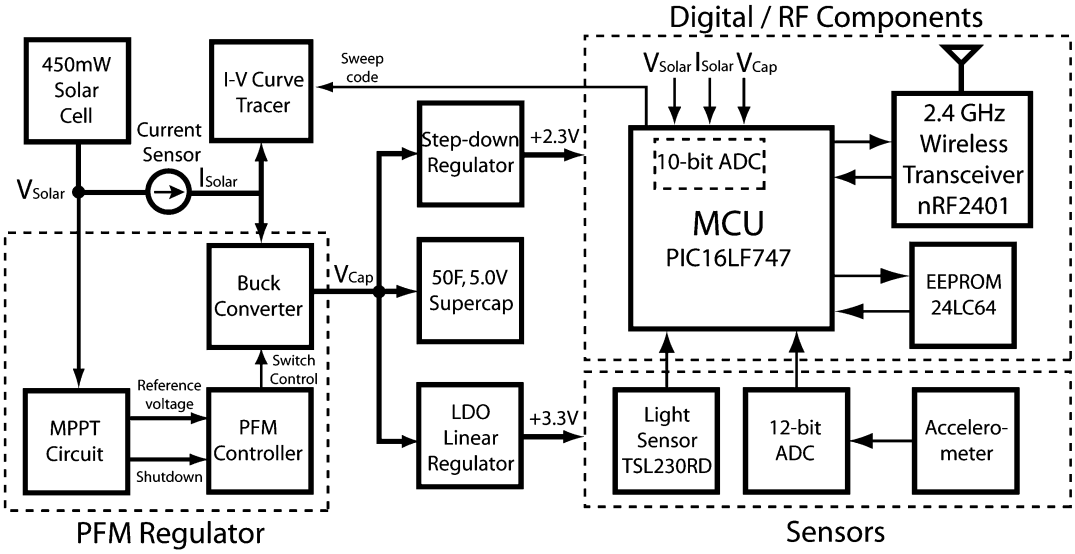

Fig. 3. Everlast system block diagram.

Therefore, the MPP can be approximated by the two following equations:

$$V_{\mathrm{mp}} \approx K_{V_{\mathrm{mp}}} V_{\mathrm{oc}} \tag{7}$$

$$I_{\mathrm{mp}} \approx K_{I_{\mathrm{mp}}} I_{\mathrm{sc}}. \tag{8}$$

B. MPPT Approaches

Numerous methods proposed to date for tracking the MPP of solar cells include using a solar cell model, hill-climbing, open-circuit solar voltage, and short-circuit solar current [6]–[9].

A solar cell model would require measuring sunlight intensity and temperature to generate optimal voltage and current by a microprocessor either locally or on a remote PC. A lookup table could be used locally by a low-power MCU as well; however, in both conditions the tracker would require light and temperature sensors and an accurate solar cell model [10].

An easier approach with guaranteed accuracy is the brute force hill-climbing technique. It entails sweeping solar voltage while measuring the current. The disadvantage is that it requires continuous sampling and a great deal of dedicated circuitry in the form of a DSP, FPGA, or MCU to calculate the optimal power point. The power and cost to run those chips are too high to keep the converter efficient and cost effective for a sub-Watt power source.

With a $\pm 5\%$ accuracy needed, the first two approaches are not necessary and would end up consuming too much power in any case. In the next two tracking methods, the voltage and current at MPP are directly proportional to the open-circuit voltage and short-circuit current, as described by (7) and (8), respectively [11], [12]. The short circuit method entails shorting the solar cell and measuring the short circuit current, which directly determines the MPP [11]. The open-circuit voltage method simply requires disconnecting the solar cell from any load and measuring the open-circuit solar voltage, which again is directly related to the MPP [12], [13]. Both methods would simply require the regulator to shut down for a few moments to measure the open-circuit voltage or short-circuit current, calculate the new operating point, and feed that value into the regulator. With these techniques, MPP can be reached more quickly since it requires only a single computation and a momentary shutdown of the converter. The new operating point can be held by analog sample-and-hold circuitry, which further simplifies the design. Both methods are not as accurate as the hill climbing method, but the complexity and overhead power make hill climbing inefficient.

Mutoh and Inoue [14] proposes to charge series-connected ultraelectric double-layer capacitors while combining MPPT. This would be the most similar to our work here, except it is designed for a much larger scale system that inverts the dc power in the supercapacitor and feeds it into the electric grid. Their objective thus is the overall transfer efficiency, but they cannot minimize the absolute overhead level of their MPPT.

III. Everlast System Design

Fig. 3 shows an overview of the Everlast design. The system is designed for three primary tasks: charging the capacitor using a pulse-frequency modulated (PFM) regulator, feeding the PFM controller the optimal operating point for the solar cell, and all the typical WSN functions including reading sensor data and communication with nodes and base-stations through the wireless transceiver. Since the supercapacitors have a much higher power density than a battery, it can power sensors that batteries with similar energy capacities could not. In cases where the sensor is only momentarily on and has low average power consumption but high peak power, a small supercapacitor can satisfy the power requirements and offer a very small form factor.

A. PFM Regulator

Since the capacitor is seen as a short to the solar cell when they are connected together, the traditional high-efficiency voltage regulator such as the PWM dc–dc converter would not function properly because V_{solar} would quickly fall to V_{cap} and greatly deviate from V_{mp}. This is primarily caused by the internal resistance for a sub-Watt solar cell or wind generator being on the order of hundreds of ohms while the supercapacitor ESR in the single-digit milliohm range. This impedance mismatch between the power source and capacitive load of four to five orders of magnitudes, and six to seven orders of magnitudes with a piezoelectric generator, necessitates momentarily

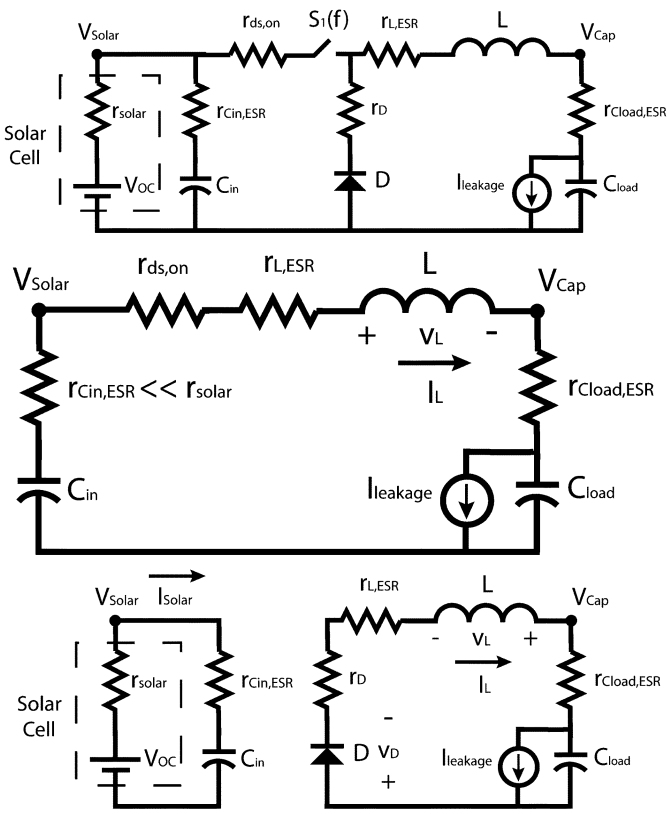

Fig. 4. PFM Regulator: (a) circuit implementation, (b) switch on, and (c) switch off. $C_{\rm in} = 1\ \mu$F, $S_1 =$ Fairchild FDN358P, $L = 100\ \mu$H, $C_{\rm load} =$ 50 F, 5.0 V.

closing the switch in a series of pulses so that $V_{\rm solar}$ remains at $V_{\rm mp}$.

As shown in Fig. 4, the PFM regulator initially appears to be an ordinary buck regulator with a capacitive rather than resistive load. Due to the capacitive load and pulse frequency modulation, the regulator behaves both as a switched-capacitor and buck regulator. Fig. 5 presents a PFM regulator simulation to further describe the regulator in operation. A large 10 μF input capacitance and small 10 μF capacitive load are used in simulation to better illustrate the charging process, though a smaller input capacitor and larger output capacitor would be used in reality. At startup, switch S_1 is open, and the solar cell charges the input capacitor, $C_{\rm in}$. At t_0, $V_{\rm solar}$ reaches the upper threshold of (9), which is set by the PFM controller

$$V_{\rm mp} - V_{\rm hyst} < V_{\rm solar} < V_{\rm mp} + V_{\rm hyst} \tag{9}$$

S_1 is then closed and $C_{\rm in}$ sends current to the inductor, L, and the supercapacitor, $C_{\rm load}$, similar to a switched-capacitor regulator. Since $r_{\rm Cin,ESR}, r_{\rm Cload,ESR}$, and $r_{\rm L,ESR}$ have a much lower combined impedance than the solar cell, $C_{\rm in}$ discharges much quicker than the time it charges back up to the upper threshold. This results in a high current pulse charge to $C_{\rm load}$ at least an order of magnitude higher than the average $I_{\rm solar}$ current with a pulse width too short for a PWM regulator to generate. At t_1, the pulse ends when $C_{\rm in}$ meets the bottom threshold in (9) at which time it starts to recharge up to the upper threshold. Concurrently, the inductor reverses

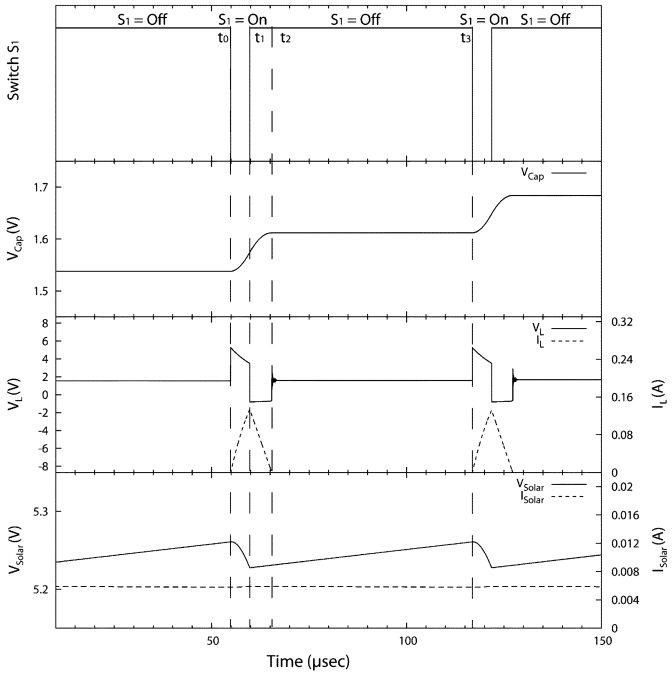

Fig. 5. PFM regulator simulation- $C_{\rm in} = 10\ \mu$F, $L = 100\ \mu$H, $C_{\rm load} =$ 10 μF.

polarity and transfers its remaining energy to $C_{\rm load}$ through the free-wheeling diode, as in a normal buck regulator, until it is completely discharged at t_2. At $t_3, C_{\rm in}$ is charged back to the upper threshold and the regulator has returned to the same state as t_0, thus completing a single PFM charge cycle. The circuit is similar to a switched-capacitor circuit in that it charges a capacitor and then transfers that energy to the output load capacitor. The only difference is that an inductor is added to buffer the voltage difference between $V_{\rm solar}$ and $V_{\rm cap}$. The pulse frequency indirectly depends upon the thresholds for switching the regulator as well as the solar power at any given time because more solar power allows $C_{\rm in}$ to be charged more quickly and reach the top threshold sooner (9). The pulse width is dependent upon $r_{\rm Cin,ESR}$ and $r_{\rm Cload,ESR}$.

Assuming $\Delta V_{\rm hyst} \ll V_{\rm solar}$ and neglecting $I_{\rm solar}$ for the moment, $C_{\rm in}$ can be treated as a voltage source from $t_0 < t < t_1$ as shown in Fig. 4(b).

The circuit is then described as a simple RLC circuit and Kirchoff's voltage law can be applied [15]

$$R_{\rm esr1} = r_{\rm Cin} + r_{\rm ds,on} + r_L + r_{\rm Cload} \tag{10}$$

$$L\frac{di_L}{dt} + R_{\rm esr1} i_L + \frac{1}{C_{\rm load}} \int_{t_0}^{t_1} i_L d\tau + V_{\rm cap} = V_{\rm solar}. \tag{11}$$

Similarly, the $i_L(t)$ can be calculated when S_1 is opened at t_1

$$R_{\rm esr2} = r_D + r_L + r_{\rm Cload} \tag{12}$$

$$L\frac{di_L}{dt} + R_{\rm esr2} i_L + \frac{1}{C_{\rm load}} \int_{t_1}^{t_2} i_L d\tau + V_{\rm cap} + V_D = 0. \tag{13}$$

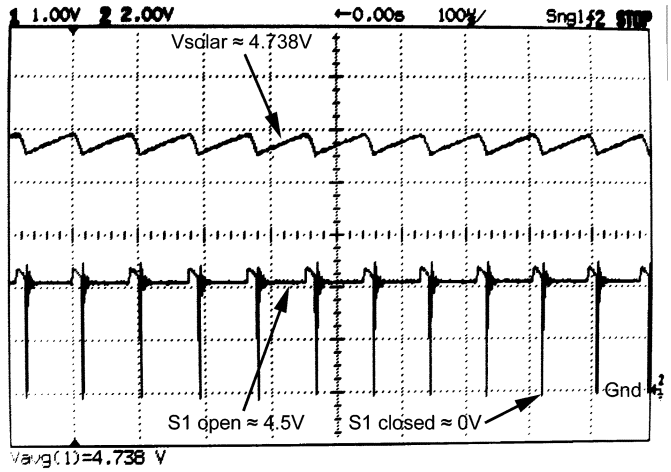

Fig. 6. PFM regulator waveform: $V_{\rm solar}$ (top), S_1 (bottom).

The pulse width time, $t_0 < t < t_1$, can be calculated as the time required to discharge $C_{\rm in}$ from the upper to lower $V_{\rm solar}$ threshold

$$t_{\rm on} = \frac{2\Delta V_{\rm hyst} C_{\rm in}}{\int_{t_0}^{t_1} i_L(t) - i_{\rm solar}(t) d\tau} \tag{14}$$

$$t_{\rm on} \propto V_{\rm hyst} C_{\rm in} R_{\rm esr1} L. \tag{15}$$

Conversely, the time that the switch is open, $t_1 < t < t_3$, is the time required to recharge $C_{\rm in}$ from the lower to upper threshold

$$t_{\rm off} = \frac{2\Delta V_{\rm hyst} C_{\rm in}}{\int_{t_1}^{t_3} i_{\rm solar}(t) d\tau} \tag{16}$$

$$t_{\rm off} \propto V_{\rm hyst} C_{\rm in} \frac{1}{i_{\rm solar}}. \tag{17}$$

Finally, using (14) and (15) the pulse frequency can be calculated as

$$f_{\rm pulse} = \frac{1}{t_{\rm on} + t_{\rm off}} \tag{18}$$

$$f_{\rm pulse} \propto \frac{1}{V_{\rm hyst} C_{\rm in}} i_{\rm solar}. \tag{19}$$

Although the PFM regulator switch S_1 closes for a short period of time, the pulse width still has a defined finite width. From (17) the pulse width is primarily set by the components in the regulator and the capacitive load. The pulse width is therefore fairly constant during operation and is generally less than 1% of the pulse period due to the large source and load impedance mismatch. Since $t_{\rm on}$ will not change much, the frequency modulation at runtime will come from varying $t_{\rm off}$. From (17) and (19), pulse frequency is largely dependent upon the PFM controller hysteresis, input capacitance, and $i_{\rm solar}$. During runtime, the pulse frequency will change in order to keep the regulator within the hysteresis levels set in the PFM control circuitry. Fig. 6 shows the solar voltage and pulses sent to the switch when the regulator is operating. As explained earlier, $V_{\rm solar}$ is kept within the bounds set by (9).

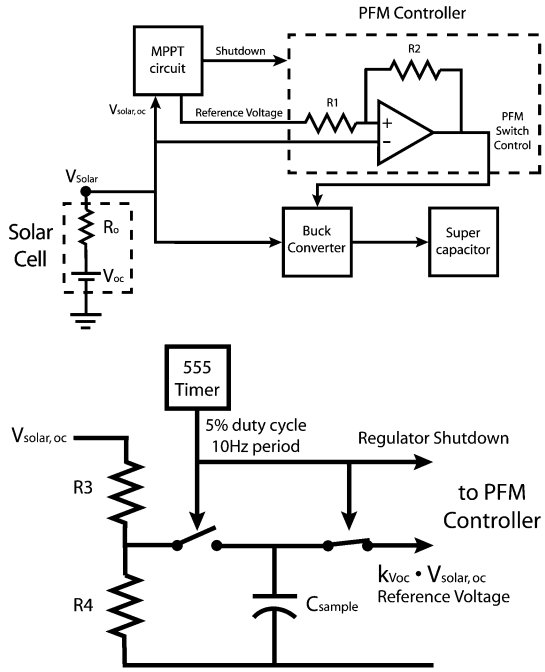

Fig. 7. (a) PFM Controller and (b) dc sweep circuitry.

B. PFM Controller and MPP Tracking

The function of the PFM controller is to pulse the buck regulator every time $V_{\rm solar}$ exceeds the specified reference voltage. Fig. 7(a) shows $V_{\rm solar}$ being compared to a reference voltage from the MPPT circuitry. Hysteresis is used to control the circuit from unstable switching and set the maximum pulse frequency. Using R_1 and R_2, the hysteresis is set (20)

$$V_{\rm hyst} = V_{\rm ref} \frac{R_1}{R_1 + R_2} \tag{20}$$

$$k_{V_{\rm mp}} = \frac{R_4}{R_3 + R_4} \tag{21}$$

$$V_{\rm mp} = k_{V_{\rm mp}} \cdot V_{\rm solar,oc} = \frac{R_4}{R_3 + R_4} \cdot V_{\rm solar,oc}. \tag{22}$$

The PFM controller requires a reference voltage in order to keep $V_{\rm solar}$ at $V_{\rm mp}$. Amongst the various MPP tracking methods to find the optimal solar voltage, open-circuit and short-circuit tracking have the simplest implementation, lowest power overhead, and quickest calculation time. These advantages come at the cost of accuracy in comparison to the hill-climbing method; however, in order to minimize the power overhead in sub-Watt power sources some reduction in accuracy is necessary. In fact, the power overhead from extra circuitry in hill-climbing method consisting of a microcontroller or DSP chip will certainly outweigh the increased power output from the sub-Watt solar cell with more accurate tracking.

As discussed earlier, the open-circuit voltage tracking requires multiplying open-circuit solar voltage, $V_{\rm solar,oc}$, by a constant $k_{V_{\rm mp}}$ (7). $V_{\rm solar,oc}$ is obtained by electrically disconnecting any load, such as the PFM regulator, from the solar cell so that the open-circuit voltage can be measured. In short-circuit current tracking, $I_{\rm solar,sc}$ is measured by shorting the solar cell to ground and measured the short-circuit current. The constants, $k_{V_{\rm mp}}$ and $k_{I_{\rm mp}}$, can be measured experimentally or found in a

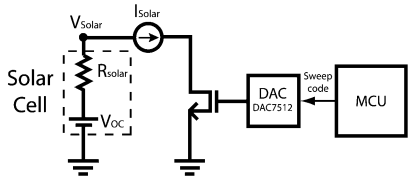

Fig. 8. I–V curve tracer circuit.

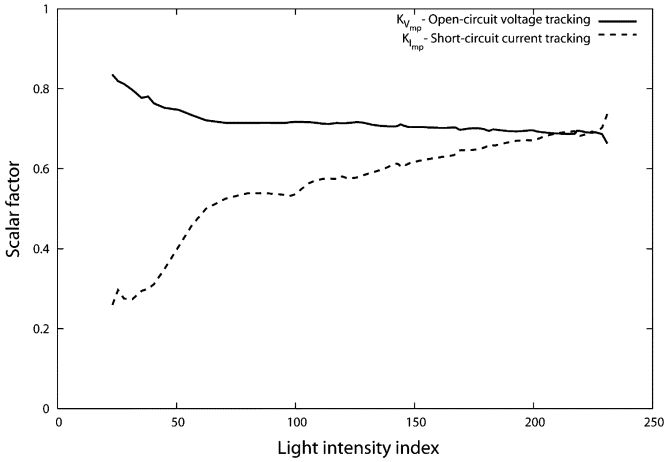

Fig. 9. Voltage and current tracking constants calculated over one day on SolarWorld SPE-50-6 450 mW Solar Panel.

model of the solar cell. Since these constants are themselves dependent upon multiple variables including solar irradiance, angle of solar incidence, temperature, etc., an I–V curve tracer is used to experimentally find these values and observe the linearity of the constants. Throughout the day I–V curve traces similar to Fig. 2 were generated on the Everlast board using the circuit described in Fig. 8. The gate voltage of the n-channel FET is swept using a DAC and $I_{\rm solar}, V_{\rm solar}$ points are saved to the EEPROM. Using the MCU on board, $P_{\rm solar}$ is calculated and the hill-climbing technique is used to traverse the power vs. voltage curve to find the $V_{\rm mp}$ and $I_{\rm mp}$ as well as $V_{\rm solar,oc}$ and $I_{\rm solar,sc}$. Across a relative light intensity, the constants are then shown in Fig. 9. Voltage tracking is preferred because under normal lighting conditions $K_{V_{\rm mp}}$ is between 0.68–0.72 and reaches up to 0.80 in low light conditions. This is much better than the wide swing range of the current tracking constant. The open-circuit voltage can also be easily implemented by periodically shutting down the regulator with a timer and then sampling the voltage with an ADC or sample-and-hold circuit.

As illustrated in Fig. 7(b), the 555 timer shuts down the PFM regulator for 5 ms every 100 ms and signals the sample-and-hold circuit to sample the reference voltage. Since $k_{V_{\rm mp}}$ is less than 1.0, it can be set with two resistors (21). $V_{\rm mp}$ is then the voltage division of $V_{\rm solar,oc}$ through the resistive divider (22). At 10 Hz, the tracker can keep up during fast-changing environmental conditions such as partially cloudy weather. Fig. 10 shows how the solar voltage periodically jumps up to the open circuit value when the regulator is shut down and then the regulator restarts with the updated $V_{\rm mp}$ value.

Finally, the power-on reset circuits (not shown) are used to prevent overcharging the supercapacitors above 5.0 V and

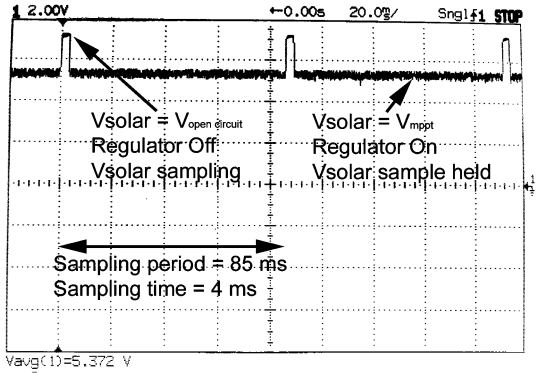

Fig. 10. Open-circuit voltage MPP tracking.

turning on the Everlast sensor node circuitry until the supercapacitor is charged up to 2.4 V. The PFM regulator and MPP tracker circuitry are all powered solely by the solar cell and can charge the supercapacitor from a dead-start.

C. WSN Functions

Although the primary goal of Everlast is to keep the solar cells at MPP and operate for 20 years, some of the latest technologies in MCUs, sensors, and transceivers are adopted so that the board will operate with lower power requirements. As shown in Fig. 3, the digital and RF components operate on a lower supply rail than the sensors. The MCU, EEPROM, and transceiver operate at a reduced 2.3 V supplied by a step-down PWM regulator and the sensors are powered by a 3.3 V linear regulator to help minimize noise to sensitive electronics.

The PIC16LF747 is selected as the MCU because of its low supply current from 25 μA at 31.25 kHz to 930 μA at 8 MHz with $V_{\rm DD}$ at 3.0 V using an internal RC oscillator. The MCU can operate from 2.0 V to 5.5 V and the internal RC oscillator can be controlled at runtime. There has been much work on dynamic voltage and frequency scaling (DVFS), and practically any of those techniques can be written into the firmware.

The low-power Nordic nRF2401 2.4 GHz GFSK Transceiver is used for wireless communications. Operating in the 2.4 GHz ISM band, it supports 125 channels and can support a dense network of sensor nodes. With the ability to send ShockBurst messages, the transceiver turns on to send a 256-b packet in a 1 Mbps data-stream and quickly goes back to standby. With 0 dBm RF power, the transceiver has line of sight (LOS) range of 300 m according to the datasheet, and we have physically verified it for at least a 150 m LOS range. With an integrated pseudo-MAC layer, the transceiver incorporates a 16-b CRC and the recipient's address into the packet, eliminating the need to error check packets by the MCU.

Most sensors today either produce an analog voltage, PWM signal, or PFM signal. The MCU can read the first using its internal 10-b ADC or through a four-channel 12-b ADC on board. The latter two signals can be measured with an internal timer/counter built in the MCU. The TSL230RD light sensor improves upon traditional methods of measuring light intensity such as with a photodiode, because it has a pin-selectable light aperture such that a greater dynamic range of light can be measured. The light sensor draws 2 mA when operating, but since it generates a square-wave output, the MCU can easily count

the edges using the internal counter in a matter of 1–2 ms while consuming less than 12 μJ per sampling. The ADXL202 is a dual-axis ± 2 g accelerometer consuming 600 μA. The supply current is low enough that the MCU I/O pin can power it during sampling and power it down otherwise. The remaining ADC pins are drawn out to the board so that additional sensors can be added anytime. The board also includes an EEPROM that can be used for storing sensor data (see Fig. 16).

IV. Experimental Results

Three metrics determine the performance of the Everlast board: efficiently charging the supercapacitor, tracking the solar cell at MPP, and running continuously for 24 h a day.

A. MPPT Efficiency of PFM Regulator

The regulator efficiency is measured with a test setup that is similar to the intended operational setup but is also easily reproducible. A solar cell is placed under a high-power, adjustable halogen lamp that can provide a constant solar irradiance in a laboratory environment as shown in Fig. 17. The solar cell sends power to the PFM regulator to charge two 10 F supercapacitors in series with an equivalent capacitance of 5 F, 5 V. A SolarWorld SPE-50-6 450 mW solar cell with $V_{\rm mp}$ between 4.5–6 V is used. This setup provides a typical deployment of the Everlast sensor node, and save for ambient temperature differences, should provide accurate measurements.

Since it is not easy to measure the energy transferred in a single pulse without a high-speed digitizer, the next best solution is to charge the supercapacitors from depletion to full charge while measuring the average $V_{\rm solar}$, $I_{\rm solar}$, and $V_{\rm cap}$ with the ADC on board the sensor node. The efficiency is calculated by charging the capacitor from 0 to 4.9 V and comparing the energy output by the solar cell with the increase in the capacitor's energy level from the start to the end of charging

$$\eta_{\rm Reg} = \frac{E_{\rm solar}}{E_{\rm cap,end} - E_{\rm cap,start}} = \frac{P_{\rm solar,avg} \cdot t_{\rm chargetime}}{0.5C\left(V_{\rm end}^2 - V_{\rm start}^2\right)}. \quad (23)$$

Fig. 11 shows the overall regulator efficiency as measured across varying solar power, and generally over 40 mW the efficiency plateaus. At lower solar power, the 2 mW power overhead from the control circuitry heavily taxes the input power and the shrinking solar current has to offset the input capacitance leakage current. Fig. 12 provides further insight into the regulator across varying capacitor voltage. In the initial moments of charging a dead capacitor, the voltage difference between the solar cell and capacitive load is the largest and ramps up to a larger peak current leading to larger voltage drops across the ESR in the regulator components. Since the sensor is assumed to be online all the time, which means being charged to at least 3 V, this scenario is unlikely to occur frequently. Towards the end of the charging phase, the capacitor reaches the solar voltage and the inductor voltage decreases. The smaller inductor voltage causes the pulse current to ramp up slower and widen the pulse width. The regulator switch S_1 is now on longer, leading to more loss in the regulator components.

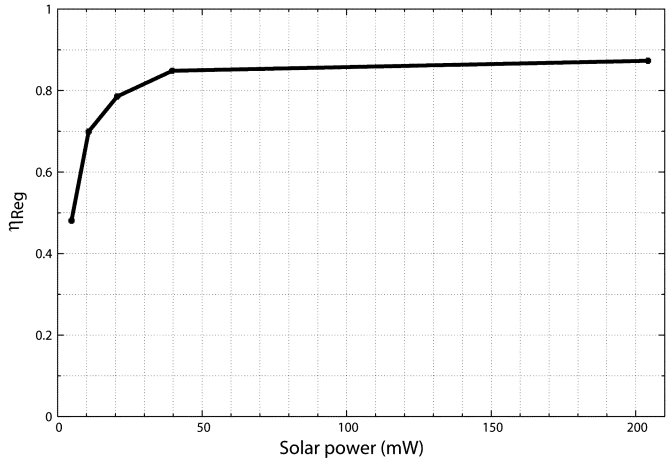

Fig. 11. PFM regulator efficiency versus solar power.

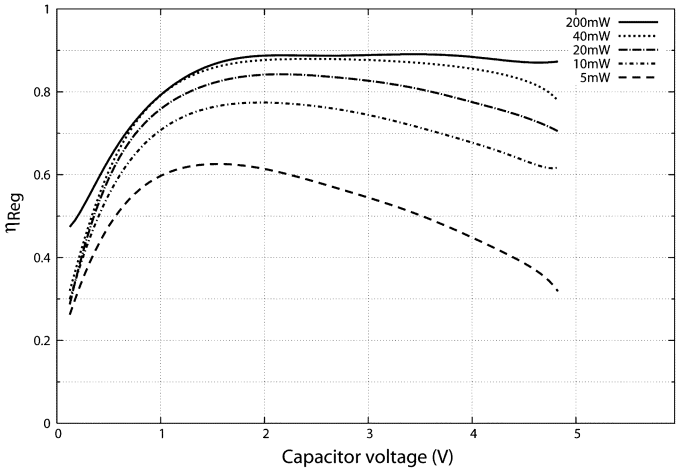

Fig. 12. PFM regulator efficiency versus capacitor voltage.

The regulator as it stands operates above 80% efficiency at solar power over 20 mW and can still harvest power down to 5 mW. The PFM controller and MPPT tracker circuitry are simple enough that they only consume 2 mW. In comparison, lithium-ion and NiMH switch-mode battery chargers require a few hundred milliwatts of power to operate efficiently and requires 10 mW for the complex control circuitry. This constraint for battery-powered sensor nodes requires that at least a 400 to 500 mW solar cell be used whereas Everlast can currently operate with a smaller 100 mW solar cell. Everlast can then fit in a smaller form factor and reduce the overall cost. Appreciable gains can still be made at lower power levels by replacing the diode with an n-channel FET for synchronous rectification and using low-power comparators in the control circuitry. For power sources less than 10 mW such as the stamp-sized solar cells and piezoelectric generators, a lower-leakage 0.1 to 10 F supercapacitor would be the ideal energy storage available today.

B. Efficiency of Solar-Charging a Supercapacitor

Fig. 13 shows a comparison of charging two 10 F supercapacitors in series directly from the solar cell and charging through the PFM regulator. Since Everlast can calculate and set the solar

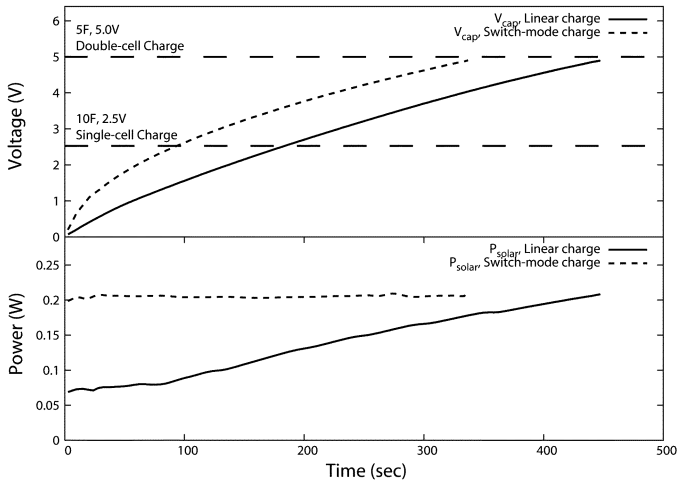

Fig. 13. Comparison between direct capacitor charging and PFM-regulated charging.

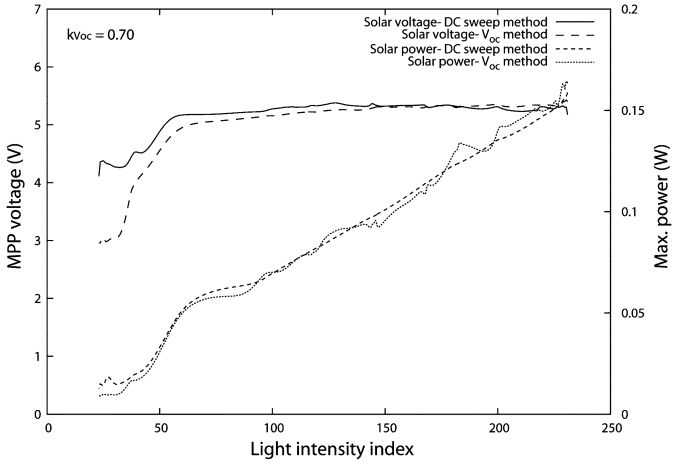

Fig. 14. MPPT comparison between dc sweep and $V_{\rm oc}$ method-$V_{\rm solar}$ (top), $P_{\rm solar}$ (bottom).

cell to the maximum power point, it is able to generate more power right from the start of the charge cycle. The power generated from a direct solar charge changes as the supercapacitor is charged. Since the supercapacitor forces $V_{\rm solar}$ down to the supercapacitor voltage, the solar cell cannot generate the 200 mW peak power which occurs at a $V_{\rm mp}$ of 5.2 V in this test setup. The MPPT circuit sets the $V_{\rm mp}$ to 5.2 V at runtime and allows the PFM regulator to charge the supercapacitors to 5 V nearly 25% faster. When the average $V_{\rm mp}$ is higher than the supercapacitor voltage, the PFM regulator yields even better results as shown when the supercapacitor is charged to 2.5 V resulting in 100% faster charge time than the direct charge method. This observation is particularly useful if the Everlast board is running from a single 2.5 V supercapacitor that is stepped up to 3 V for the sensor node. It is also important to realize this when higher power requirements necessitate a larger solar cell, which normally has higher operational voltages where $V_{\rm solar,oc}$ is 12 to 24 V and $V_{\rm mp}$ is 9 to 18 V. In this situation, charging a 2.5 to 5 V supercapacitor through the PFM regulator would yield a 300% to 400% faster charge time over direct charging.

The PFM regulator is only useful if the MPPT circuit can feed the PFM controller the correct $V_{\rm mp}$ value. Fig. 14 shows that the voltage tracking method, with $K_{V_{\rm mp}}$ fixed at 0.70, can track solar power very closely to the hill-climbing method but without the need for an MCU/DSP. The solar cell only needs to be shutdown for 5 ms every 100 ms to sample the open-circuit solar voltage as shown in Fig. 10. The overall voltage tracking method has a tracking error of less than 5% in normal lighting conditions and less than 11% in low lighting conditions in comparison to the hill climbing method. The tracking error increases in low lighting conditions because the solar cell's $K_{V_{\rm mp}}$ reaches 0.80 while the voltage tracking constant is still fixed at 0.70 in the tracking circuitry.

If better accuracy is needed, additional circuitry can be added in the tracking circuit to compensate $K_{V_{\rm mp}}$ for changing light conditions and temperature [10]. A temperature sensor can also be added to shift $K_{V_{\rm mp}}$ up or down, though with additional overhead. The current design meets the $\pm 5\%$ accuracy goal established earlier and is achieved with a 2 mW overhead to power both the MPPT and PFM controller circuitry. The more accurate hill-climbing method could also be implemented with a low-power MCU with a similar 2 mW power consumption. However, a single accurate sweep takes more than a second by the I–V curve tracer circuit shown in Fig. 8. Since fast moving weather conditions such as cloudy skies can change $V_{\rm mp}$ in a fraction of a second, hill climbing would actually yield lower accuracy in those situations. This level of accuracy is acceptable for sub-Watt solar power generation since the voltage tracking method can be implemented with a few inexpensive, discrete components and the power requirements to operate a more accurate tracker would outstrip the increase in power generation.

TABLE II
SAMPLE POWER MODES AND CONTINUOUS RUNTIMES FROM FULLY-CHARGED 50 F, 5 V SUPERCAPACITOR AND TRANSCEIVER IN 1 MBIT/S SHOCKBURST MODE

Profile	MCU Core Freq. (MHz)	Transceiver (bps)	P_{supply} (mW)	Runtime (hrs)
p1	Sleep	20	0.68	138
p2	4.0	20	1.49	79.3
p3	4.0	51,200	5.77	22.1
p4	4.0	39,300	4.77	25.1
p5	2.0	22,500	3.37	35.4
p6	1.0	11,400	2.49	44.8
p7	4.0	Rx mode	52.4	2.2

C. Four-Day Stress Test

Everlast can efficiently charge supercapacitors from raw solar power and maximize solar power output with little power overhead. Unfortunately, the lower energy density and higher leakage current in comparison to batteries require that the sensor node minimizes power consumption during normal operation and especially in sleep mode. In the absence of solar power, Everlast must be able to run for a few days with reasonable amounts of processing power and radio activity. Creating a few sample modes in Table II, the sensor node is attached to a fully charged 50 F, 5 V supercapacitor and the runtime is measured until the $V_{\rm cap}$ drops to 2.4 V. In p1 sleep mode, the MCU turns on once a minute, measures some data from the

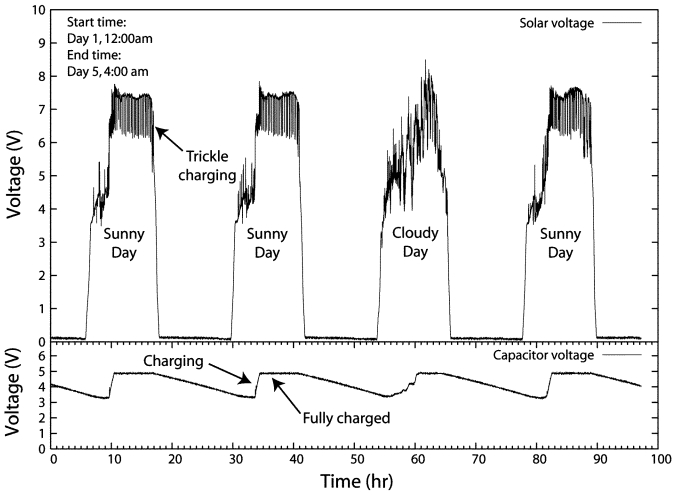

Fig. 15. Four-day 100-h outdoor stress test in P3 mode.

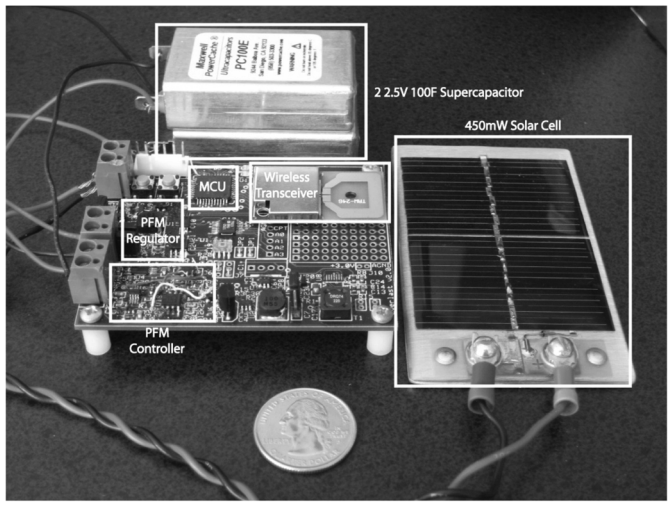

Fig. 16. Everlast prototype board.

sensors, sends out a few packets, and returns to sleep. P1 mode is very similar to sensor nodes that lie dormant most of the time and occasionally power on shortly before returning to sleep. The board was able to operate for nearly 6 days in this mode and with most of the power being consumed by leakage current in the step-down regulator, which leaves some headroom for further improvements. Mode p2 is similar to p1 except the MCU is in a busy loop at 4 MHz clock frequency. Mode p3 is similar to the capabilities of a Mica2 mote in terms MCU processing power and radio bit-rate. In p7 mode, the transceiver is in receive mode and clearly 50 F is not sufficient for the radio to be operating continuously. Fortunately, Everlast is scalable so that different solar cells and supercapacitors can be used as long as $V_{\rm mp} \geq V_{\rm cap,max}$ so that the PFM buck regulator can operate correctly. Overall, in its current configuration Everlast can operate better than nodes that normally stay in sleep mode and with two 350F supercapacitors can operate similar to the Mica2 Mote in terms of RF bandwidth and processing power with an added benefit of a 10 to 20 year operational lifetime. With further effort to reduce the leakage current, the sleep mode power consumption can be reduced, allowing the node to stay asleep off fully charged supercapacitors for a few weeks.

Fig. 15 is a stress test of Everlast running in p6 mode on a building rooftop draining the capacitor at night and recharging during the day. In fact, all the data generated in the graph are sampled by the on-board ADC and transmitted from the sensor node itself to a base station. Taking a close look at the graph, throughout the night, the capacitor is drained, and during the morning, the PFM regulator turns on and charges the capacitor. By high noon, the capacitor is fully charged at 4.9 V, and the PFM regulator is shut down, causing the solar voltage to jump to $V_{\rm oc}$. During the day, the sensor node is still transmitting data and draining power from the capacitor. Once $V_{\rm cap}$ dips below 4.85 V, the MCU restarts the regulator to recharge the capacitor back to full capacity. The third day was partly cloudy and the MPPT circuitry continuously adjusts the solar voltage to maximize the output in response to the rapid changes in solar irradiance.

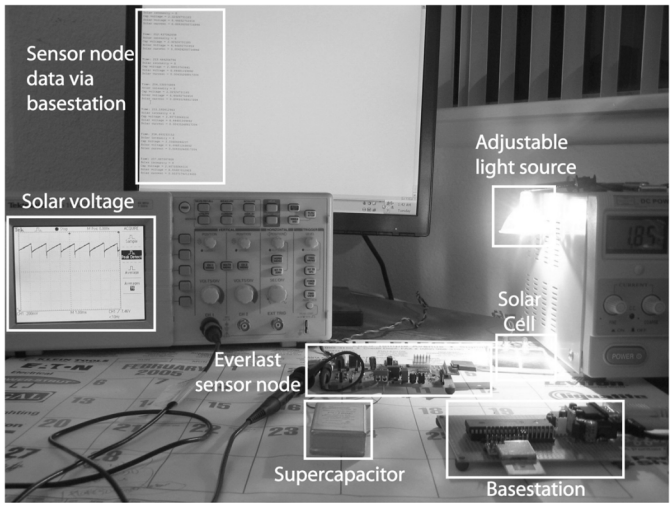

Fig. 17. Indoor experimental test setup.

V. Conclusion

This article demonstrates the feasibility of efficient energy harvesting for sub-Watt, small-scale systems combined with durable energy storage in the form of supercapacitors, which are expected to last for 20 years at non-trivial power levels. Previous maximum power point tracking systems were designed for large systems that optimize for conversion efficiency, but for small wireless sensor nodes, it is critical to maximize absolute converted power by minimizing MPPT overhead. Previous works that rely on feedback-based regulation will fail to properly charge a supercapacitor. Everlast addresses both problems by its novel feed-forward, pulse frequency modulation regulator design. We chose an open-circuit voltage MPPT scheme that achieves over 89% conversion efficiency. It may be less accurate, but its low complexity makes it suitable for small, low-power systems. Our system also charges the same supercapacitor to 5 V 25% faster, to 2.5 V 100% faster, and to even higher voltage 300% to 400% faster than direct charging. Everlast also passed multi-day stress tests while performing a

variety of wireless sensing tasks under different weather conditions. Future work includes fine-tuning of the present design to achieve higher efficiencies at lower solar power levels, further reducing the sleep mode power consumption, and further scaling onto an SoC to operate as a micro-Watt sensor node.

REFERENCES

[1] Maxwell Technologies, "BCAP0350 Datasheet," Tech. Rep., Jun. 2007 [Online]. Available: http://www.maxwell.com

[2] X. Jiang, J. Polastre, and D. Culler, "Perpetual environmentally powered sensor networks," in *Proc. 4th Int. Conf. Inform. Process. Sensor Networks*, Apr. 2005, pp. 463–468.

[3] H. Pollock, "High efficiency, high frequency power supplies for capacitor and battery charging," in *Proc. IEEE Colloq. Power Electron. Demanding Appl.*, Apr. 1999, pp. 901–910.

[4] R. Nelms and J. Schatz, "A capacitor charging power supply utilizing a ward converter," *IEEE Trans. Ind. Electron.*, vol. 39, pp. 421–428, Oct. 1992.

[5] D. King, J. Kratochvil, and W. Boyson, "Field experience with a new performance characterization procedure for photovoltaic arrays," in *Proc. 2nd World Conf. Exhib. Photovol. Solar Energy Conversion*, 1998 [Online]. Available: http://www.osti.gov/energycitations/product.biblio.jsp?osti_id=629484

[6] K. Hussein, I. Muta, T. Hoshino, and M. Osakada, "Maximum photovoltaic power tracking: An algorithm for rapidly changing atmospheric conditions," *Proc. Inst. Elect. Eng.*, pp. 59–64, Jan. 1995.

[7] C. Hua and C. Shen, "Study of maximum power tracking techniques and control of DC/DC converters for photovoltaic power system," in *Proc. IEEE PESC. Conf.*, 1998, pp. 86–93.

[8] E. Koutroulis, K. Kalaitzakis, and N. Voulgaris, "Development of a microcontroller-based, photovoltaic maximum power point tracking control system," *IEEE Trans. Power Electron.*, vol. 16, no. 1, pp. 46–54, Jan. 2001.

[9] Y. Kuo, T. Liang, and J. Chen, "Novel maximum-power-point-tracking controller for photovoltaic energy conversion system," *IEEE Trans. Ind. Electron.*, vol. 48, no. 3, pp. 594–601, Jun. 2001.

[10] D. King, J. Kratochvil, and W. Boyson, "Temperature coefficients for PV modules and arrays: Measurement methods, difficulties, and results," in *Proc. 26th IEEE Photovolt. Spec. Conf.*, Oct. 1997, pp. 1183–1186.

[11] T. Noguchi, S. Togashi, and R. Nakamoto, "Short-current pulse-based maximum-power-point tracking method for multiple photovoltaic-and-converter module system," *IEEE Trans. Ind. Electron.*, vol. 49, no. 1, pp. 217–223, Feb. 2002.

[12] J. Enslin, M. Wolf, D. Snyman, and W. Swiegers, "Integrated photovoltaic maximum power point tracking converter," *IEEE Trans. Ind. Electron.*, vol. 44, no. 6, pp. 769–773, Dec. 1997.

[13] D.-Y. Lee, H.-J. Noh, D.-S. Hyun, and I. Choy, "An improved MPPT converter using current compensation method for small scale PV-applications," in *Proc. IEEE 18th Annu. Appl. Power Electron. Conf. Expo.*, Feb. 9–13, 2003, vol. 1, pp. 540–545.

[14] N. Mutoh and T. Inoue, "A control method to charge series-connected ultraelectric double-layer capacitors suitable for photovoltaic generation systems combining mppt control method," *IEEE Trans. Ind. Electron.*, vol. 54, no. 1, pp. 374–383, Feb. 2007.

[15] R. W. Erickson and D. Maksimovic, *Fundamentals of Power Electronics*, 2nd ed. Norwell, MA: Kluwer, 2001.

Farhan I. Simjee (M'06) received the B.S. degree in electrical engineering and computer engineering and the M.S. degree in electrical and computer engineering from the University of California, Irvine, in 2004 and 2006, respectively.

He is currently a Hardware Engineer with the European Aeronautic Defence and Space Company (EADS), Schiphol-Rijk, The Netherlands, involved in designing test and measurement equipment. His research interests include low-power embedded systems, wireless sensor nodes, and renewable energy harvesting.

Pai H. Chou (M'04) received the A.B. degree from the University of California, Berkeley, in 1990, and the M.S. and Ph.D. degrees from the University of Washington, Seattle, in 1993 and 1998, respectively.

He is an Associate Professor at the University of California, Irvine, USA and at the National Tsing Hua University, Hsinchu, Taiwan, R.O.C. His research interests include hardware/software codesign of embedded systems, low-power design, and wireless embedded sensing systems.

Dr. Chou received the NSF CAREER Award and is a member of ACM. He served as Program Co-Chair for the First IEEE/ACM/IFIP Conference on Hardware/Software Codesign and System Synthesis (CODES+ISSS'03) and General Co-Chair in 2004.